Fragmentation of C_{70} in Valence Ionization

H. Katayanagi[1,2], B. P. Kafle[2], T. Mori[1], J. Kou[1], K. Mitsuke[1,2], Y. Kubozono[3]

[1]*Department of Vacuum UV Photo-Science, Institute for Molecular Science, Okazaki 444-8585, Japan*
[2]*Graduate University for Advanced Studies, Okazaki 444-8585, Japan*
[3]*Department of Chemistry, Okayama University, Okayama 700-8530, Japan*

In the electron impact [1] and photo [2] ionization processes of the C_{60} molecules, fragment ions such as C_{60-2n}^{z+} ($n = 1, 2 \ldots$; $z = 1, 2 \ldots$) appear when the excess energies exceed those thermochemical thresholds of dissociative ionization by 30 – 40 eV. This is because C_{60} has a large number of internal degrees of freedom and does not have specifically weak bond to rupture owing to its highly symmetrical structure. This energy storage in the fullerenes is thus referred to as the "kinetic shift".

In our previous study [3], the fragment ion yield spectra of C_{60} in dissociative ionization by the synchrotron radiation have been recorded experimentally. From the spectra, we evaluated the appearance energies, $AE(n, z)$, which corresponds to the onset energies of ion yield spectra. The experimental values of $AE(n, z)$ were well consistent with those obtained by our RRKM calculations. The values of $AE(n, z)$ exceeded their thermochemical thresholds by 30 – 33 eV and increased by 5 – 6 eV with increasing n. From these results, we concluded that the photofragmentation of C_{60}^{z+} was governed by the mechanism of internal conversion of the electronically excited states of C_{60}^{z+}, statistical redistribution of the excess energy among a number of vibrational modes, and sequential ejection of the C_2 units.

Is this mechanism also valid in C_{70}? The C_{70} is a stable fullerene next larger in size to C_{60}. The kinetic shift can be either smaller or larger than that of C_{60}, since the C_{70} molecules have less symmetry while they have a larger number of degrees of freedom than C_{60}. To answer the question, we measured the photofragment ion yield spectra using time-of-flight mass spectrometer coupled with a monochromator at the beamline 2B in UVSOR.

Photofragment ion yields of C_{70-2n}^{2+} divided by the yield of the parent ion, C_{70}^{2+}, are shown in Fig. 1. Corresponding triply charged ion yields are also shown in Fig. 2. Note that singly charged photofragment ions were scarcely detected in whole energy range of the measurement. At the first glance, the behavior of the photofragment yield curves for $n \geq 5$ (i. e. production of smaller fragment than C_{62}^{z+}) is different from that for $n < 5$. This fact implies the carbon number of 60 is a magic number also in the photofragmentation processes.

This difference appears more clearly in energies at onsets of the yield curves, namely $AE(n, z)$. Both in doubly and in triply charged ions, the values of $AE(n, z)$ for $n < 5$ increase by approximately 7 eV with increasing n. The kinetic shift in C_{70}^{z+} is found to be 37 eV. In addition, the results of preliminary RRKM calculations in photofragment size of $n < 5$ are consistent with the experimental results. The mechanism to produce photofragments of $n < 5$ from C_{70} is, therefore, the same as that from C_{60}. Whereas the values of $AE(n, z)$ for $n > 5$ stay almost constant. This means that another mechanism should be invoked to explain the production of C_{60-2n}^{z+} in the photofragment size of $n \geq 5$. To elucidate the mechanism, we plan to perform a photoelectron photoion coincidence and a photofragment momentum spectroscopy to clarify energy partitionings during the dissociative photoionization of fullerenes.
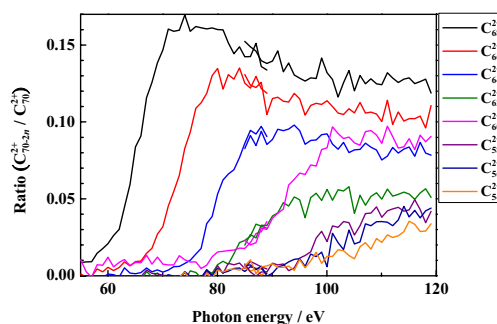
Fig. 1   Doubly charged photofragment ion yields (divided by the parent ion yield).
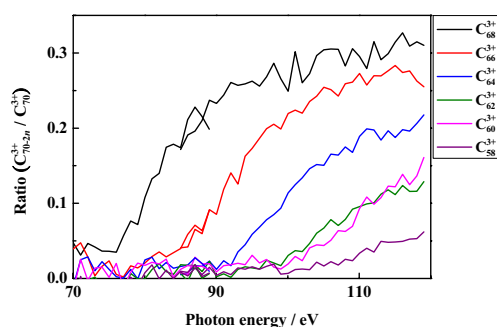
Fig. 2   Triply charged photofragment ion yields (divided by the parent ion yield).

[1] R. Wörgötter, B. Dünser, T. D. Märk, M. Foltin, C. E. Klots, J. Laskin and C. Lifshitz, J. Chem. Phys. **104** (1996) 1225.
[2] P. Wurz and K. R. Lykke, J. Phys. Chem. **96** (1992) 10129.
[3] J. Kou, T. Mori, Y. Kubozono and K. Mitsuke, Phys. Chem. Chem. Phys. **7** (2005) 119.

Photoion Yield Curves of Pr@C$_{82}$ in the Range 100 – 150 eV

H. Katayanagi[1,2], B. P. Kafle[2], T. Mori[1], J. Kou[1],
Y. Takabayashi[3], E. Kuwabara[3], Y. Kubozono[3], K. Mitsuke[1,2]

[1]*Department of Vacuum UV Photo-Science, Institute for Molecular Science,*
Okazaki 444-8585, Japan
[2]*Graduate University for Advanced Studies, Okazaki 444-8585, Japan*
[3]*Department of Chemistry, Okayama University, Okayama 700-8530, Japan*

Endohedral metallofullerenes (M$_m$@C$_n$) have attracted attention because of their possibilities of applications toward materials of novel functionalities [1]. The metallofullerenes which have a structure of M@C$_{82}$ have been used in studies on their geometrical and electronic structures, because of their availability. Their, however, had been no experimental work on the optical properties of gas phase M@C$_{82}$ in the vacuum UV and soft X-ray regions, until our report of the photoion yield curves of Ce@C$_{82}$ was published in 2005 [2].

In our work on Ce@C$_{82}$, we found a giant resonance peak which had been predicted theoretically by Wendin and Wästburg [3]. This peak originates from $4d - 4f$ dipole resonance of the Ce atom. Wendin et al. found that the calculated peak consists of a broad atomic component and an oscillation induced by a fullerene cage. Observed photoion yield curves of Ce@C$_{82}$ had structures and thus found to be affected by the interference. In the present study, we measured the photoion yield curves of metallofullerenes containing Pr which is next to the Ce in the periodic table of the elements.

The Pr@C$_{82}$ beam was generated in vacuum by sublimation of the solid sample, which was synthesized by the procedure described elsewhere [4]. The typical temperature of a sample holder was 780 K. The photoion yield was measured by means of the time-of -flight (TOF) mass spectrometry in the photon energy range 100 – 150 eV.

Figure 1 shows TOF mass spectrum of Pr@C$_{82}^{z+}$ (z = 1, 2) produced by the synchrotron radiation (124 eV). Peaks of the parent ions, Pr@C$_{82}^+$ and Pr@C$_{82}^{2+}$, are clearly observed. Small peaks of C$_{60}^+$ and C$_{60}^{2+}$ can also be recognized. The intensities of them are, however, insignificant.

Time-of-flight mass spectra of other photon energies were recorded in the same manner. Intensities of ion signals in the spectra were normalized by the photon flux. We thus extracted the yield curve of Pr@C$_{82}^{2+}$ from the normalized spectra. The yield curve of Pr@C$_{82}^{2+}$ is shown in Fig. 2. The photoabsorption spectrum of Pr atoms [5] is also shown in Fig. 2. The yield curve of Pr@C$_{82}^{2+}$ has a similar behavior to the photoabsorption spectra of Pr atoms. This fact leads us to conclude that $4d - 4f$ giant resonance does not collapse in Pr@C$_{82}$, as well as in Ce@C$_{82}$.

Closer inspection reveals characteristics of Pr@C$_{82}$. The peak position of Pr@C$_{82}^{2+}$ spectrum is higher-energy shifted and its widths is slightly narrower than that of Pr atoms. This could be described that the interference effect on the spectrum for Pr@C$_{82}$ induced by the fullerene cage is different from that for Ce@C$_{82}$. We plan to make theoretical calculations necessary for more quantitative analysis of the interference effect.
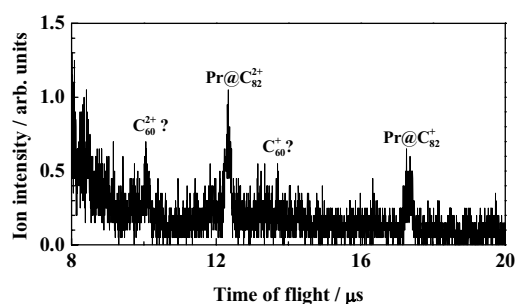
Fig. 1   TOF mass spectrum of Pr@C$_{82}^{z+}$ at the photon energy of 124 eV.
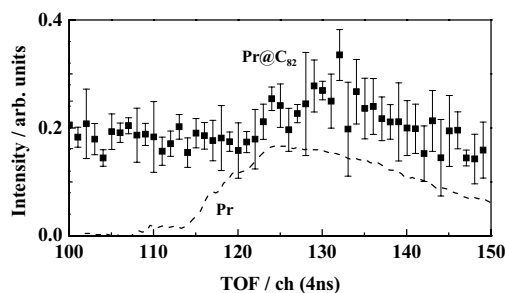
Fig. 2   Photoion yield curve of Pr@C$_{82}^{2+}$ (Filled square). Error bars indicate 1σ of values in experimental runs repeated five times. Dashed curve shows absorption spectrum of Pr atoms [5].

[1] H. Shinohara, Rep. Prog. Phys. **63** (2000) 843.
[2] K. Mitsuke, T. Mori, J. Kou Y. Haruyama and Y. Kubozono, J. Chem. Phys. **122** (2005) 064304.
[3] G. Wendin and B. Wästberg, Phys. Rev. B **48** (1993) 14764.
[4] K. Shibata, Y. Rikiishi, T. Hosokawa et al. Phys. Rev. B **68** (2003) 094104.
[5] M. Richter, M. Mayer, M. Pahler, T. Prescher, E. v. Raven, B. Sonntag and H.-E. Wetzel, Phys. Rev. A **40** (1989) 7007.

MOLECULAR SPECTROSCOPY AND DYNAMICS

Photofragmentation of Fullerenes in the Extreme UV: Ion Yield Curves for the Fragment Ions

K. Mitsuke[1,2], J. Kou[2], T. Mori[2], Y. Kubozono[3]

[1]*The Institute for Molecular Science, Myodaiji, Okazaki 444-8585, Japan.*
[2]*Graduate University for Advanced Studies*
[3]*Okayama University, Okayama 700-8530, Japan*

The C_{60} molecule with a compact structure of a truncated icosahedron exhibits an exceptionally high stability. However, mass spectrometric studies of C_{60} in combination with laser multiphoton ionization, heavy-ion excitation, or electron impact ionization have revealed that appreciable fragmentation occurs when the system gains energy in excitation and ionization processes. Decomposition of C_{60}^{z+} ($z \geq 1$) primarily formed is known to lead to fragment ions with even numbered carbon atoms (C_{60-2n}^{z+}, n=1, 2,…) via sequential loss of C_2 units from C_{60}^{z+} ions in high-vibrational states. In contrast, experimental studies of single photon excitation are very limited [1-4]. Recent results on the relative cross section of the fullerene fragments from C_{60} show that the appearance photon energies of C_{60-2n}^{+} and C_{60-2n}^{2+} are higher by 30 - 40 eV than the thermochemical thresholds for dissociative photoionization of C_{60} [2-4]. In a limited case of $C_{60} + h\nu \rightarrow C_{58}^{+} + C_2 + e^{-}$ Yoo et al. [1] have discussed this large kinetic shift in terms of unimolecular decay modelled by quasiequilibrium theory. However, they could not determine the theoretical appearance energy with a good accuracy, since a reliable value for the binding energy of C_{60}^{+} was not available at that time. Since then there has been no effort to apply quasiequilibrium theory to dissociative photoionization of C_{60} and to clarify the fragmentation mechanism of the fullerene ions to which large excess energy is initially deposited. In the present work we will discuss the detailed mechanisms of unimolecular reaction induced by equilibration of the excess energy among many density of states of the fullerene, by using the yield curves for the fragment ions obtained in a wide photon energy range.

All the measurements have been carried out at the bending magnet beamline BL2B constructed in the UVSOR synchrotron radiation facility in Okazaki, equipped with an 18 m spherical grating monochromator of Dragon type. The Experimental set-up for photoionization mass spectrometry of C_{60} has been described in details elsewhere [5,6]. Briefly a molecular beam of C_{60} was produced by heating the sample powder to approximately 680 K. Monochromatized synchrotron radiation was focused onto the C_{60} beam. The produced photoions were extracted by a pulsed electric field, mass-separated by a time-of-flight (TOF) mass spectrometer, and detected with a microchannel plate electron multiplier.

In order to normalize the ion counts the fluxes of the molecular and light beams were monitored throughout the measurement by a silicon photodiode and a crystal-oscillator surface thickness monitor, respectively.

Taking TOF mass spectra with scanning the monochromator we could measure the yield curves for C_{60-2n}^{z+} from C_{60} as a function of $h\nu$. For instance, Figure 1 illustrates the curves for C_{60-2n}^{+}. The curves for C_{60-2n}^{z+} are considered to provide fractional abundances of C_{60-2n}^{z+} within ~ 25 μs after ionization, at least around the onset region for each ion. With decreasing the size of 60-2n the appearance photon energies $AE(n,z)$ for a given z shift to higher $h\nu$ positions and the curves rise more gently towards a peak. Values of $AE(n,z)$ are found to be higher by 30 – 33 eV than the thermochemical thresholds for dissociative photoionization of C_{60} leading to C_{60-2n}^{z+}. Reinköster et al. have found similar large kinetic shifts [2] but their appearance $h\nu$ positions for $z = 1$ and 2 are higher by 2 – 8 eV than our values, probably due to their insufficient statistics. On the contrary, the appearance energies measured in electron impact ionization [7] show good agreement with our values.
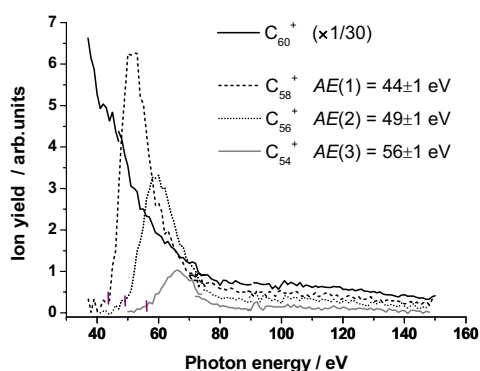
Fig. 1 Yield curves of C_{60-2n}^{+} ions (n = 1 - 3) obtained from time-of-flight mass spectra.

[1] R.K. Yoo *et al.*, J. Chem. Phys. **96** (1992) 911.
[2] A. Reinköster *et al.*, J. Phys. B **370** (2004) 2135.
[3] J. Kou *et al.*, J. Electron Spectrosc. Relat. Phenom. **144-147** (2005) 247.
[4] J. Kou *et al.*, Phys. Chem. Chem. Phys. **7** (2005) 119.
[5] J. Kou *et al.*, Chem. Phys. Lett. **374** (2003) 1.
[6] T. Mori *et al.*, Rev. Sci. Instrum. **74** (2003) 3769.
[7] P. Scheier *et al.*, Int. J. Mass Spectrom. **138** (1994) 7.

Photofragmentation of Fullerenes in the Extreme UV: Remarkably Large Kinetic Shifts of the Appearance Energies of the Fragment Ions

K. Mitsuke[1,2], J. Kou[1], T. Mori[1], Y. Kubozono[3]

[1]*The Institute for Molecular Science, Myodaiji, Okazaki 444-8585, Japan.*
[2]*Graduate University for Advanced Studies*
[3]*Okayama University, Okayama 700-8530, Japan*

We have measured the yield curves for C_{60-2n}^{z+} from C_{60} as a function of the photon energy $h\nu$ to study the mechanisms and kinetics of the unimolecular reaction of parent ions C_{60}^{z+} in high-vibrational states. Typical spectra for C_{60-2n}^{2+} are given in Fig. 1. These curves are considered to provide fractional abundances of C_{60-2n}^{2+} within ~ 25 μs after ionization, at least around the onset region for each ion.

When C_{60} is photoionized at the appearance photon energies, namely at $h\nu = AE(n,z)$, we are able to write the maximum internal energy $E_{max}(n,z)$ initially transmitted to C_{60}^{z+} as

$$E_{max}(n,z) = AE(n,z) + E_v - IP(z) \qquad (1)$$

by assuming the kinetic energy of the emitted photoelectron to be zero. Here, E_v denotes the vibrational energy of C_{60}, and $IP(z)$ is the ionization potential of C_{60} for the formation of C_{60}^{z+} (see Fig. 2). In this study, $E_v = 3.3$ eV is assumed and $IP(z)$ taken from the literature (7.6, 19.0, and 35.6 eV for $z = 1, 2$, and 3, respectively). We have evaluated $E_{max}(n,z)$ from eq. (1) and listed the resultant values in Table 1 for C_{60-2n}^{z+}. It is expected that $E_{max}(n,z)$ is nearly equal to the upper limit of the internal energies of the primary C_{60}^{z+} above which $C_{60-2n+2}^{z+}$ fragments cannot escape from further dissociating into $C_{60-2n}^{z+} + C_2$. Table 1 reveals two trends in the dependences of $E_{max}(n,z)$ on n and z of the fragments. First, the difference $E_{max}(n+1,z) - E_{max}(n,z)$ depends weakly on n, varying from 5 to 9 eV. This may reflect relatively weak n-dependences [1,2] of the binding energies for the unimolecular reaction:

$$C_{60-2n+2}^{z+} \; (n \geq 1) \rightarrow C_{60-2n}^{z+} + C_2 \qquad (2)$$
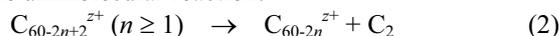
Second, $E_{max}(n,z)$ for a given n is almost unchanged irrespective of z. This remarkable finding, together with the prominent kinetic shifts, implies that internal conversion of the electronically excited states of C_{60}^{z+} results in redistribution of the excess energy among the vibrational degrees of freedom followed by successive ejection of the C_2 units, as demonstrated schematically in Fig. 2.
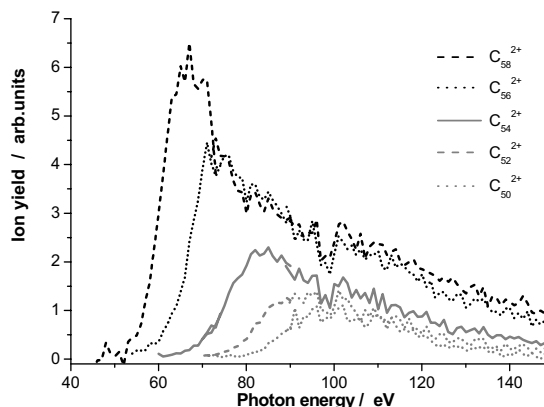
Fig. 1 Yield curves of C_{60-2n}^{2+} ions ($n = 1 - 5$) obtained from time-of-flight mass spectra.
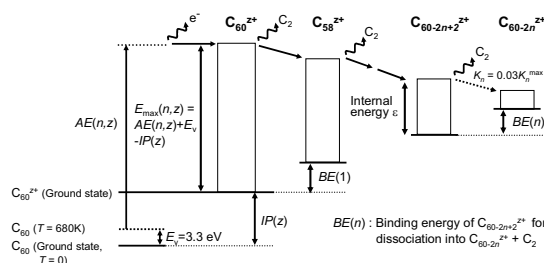
Fig. 2 Scheme of the energetics of the C_2 loss in dissociative photoionization of C_{60}.

[1] M. Foltin *et al.*, J. Chem. Phys. **98** (1993) 9624.
[2] R. Wörgötter *et al.*, J. Chem. Phys. **104** (1996) 1225.

Table 1 Upper limit $E_{max}(n,z)$ of the internal energies (eV) of the primary C_{60}^{z+} ions above which $C_{60-2n+2}^{z+}$ fragments cannot escape from further dissociating into $C_{60-2n}^{z+} + C_2$ ($n \geq 1$).

	$C_{60-2n+2}^{z+}$	C_{60-2n}^{z+}	Observed,[a] $E_{max}(n,z)$		
			$z = 1$	$z = 2$	$z = 3$
1	C_{60}^{z+}	C_{58}^{z+}	39.7±1	39.3±1	40.7±1
2	C_{58}^{z+}	C_{56}^{z+}	44.7±1	44.3±1	49.7±1
3	C_{56}^{z+}	C_{54}^{z+}	51.7±1	50.3±1	-[e]
4	C_{54}^{z+}	C_{52}^{z+}	-[e]	58.3±1	-[e]
5	C_{52}^{z+}	C_{50}^{z+}	-[e]	64.3±1	-[e]

[a] Obtained by using eq. (1) from the appearance photon energies for the formation of C_{60-2n}^{z+} from C_{60}.
[e] C_{60-2n}^{z+} fragment ions are not detectable.

Photofragmentation of Fullerenes in the Extreme UV: Analysis on the Critical Internal Energies

K. Mitsuke[1,2], J. Kou[1], T. Mori[1]

[1]*The Institute for Molecular Science, Myodaiji, Okazaki 444-8585, Japan.*
[2]*Graduate University for Advanced Studies*

We have employed the RRKM theory to derive the curves of fractional abundance (breakdown graphs) for C_{60}^{z+} and C_{60-2n}^{z+} ions ($n = 1 - 5$) as a function of the internal energy of the primary C_{60}^{z+}. The microcanonical rate constant $k_n(\varepsilon)$ for reaction

$$C_{60-2n+2}^{z+} (n \geq 1) \quad \rightarrow \quad C_{60-2n}^{z+} + C_2 \qquad (1)$$

of $C_{60-2n+2}^{z+}$ having internal excitation energy ε can be given by [1-3]

$$k_n(\varepsilon) = \frac{\alpha\, G^*(\varepsilon - E_0^n)}{h\, N(\varepsilon)} \qquad (2)$$

Here, α is the reaction path degeneracy, E_0^n is the critical activation energy for reaction (1), $G^*(\varepsilon - E_0^n)$ is the number of states for the transition state (activated complex), and $N(\varepsilon)$ is the density of states of $C_{60-2n+2}^{z+}$. For $n \geq 2$ the ε value of $C_{60-2n+2}^{z+}$ is computed under the assumption that the energy available after dissociation of $C_{60-2n+4}^{z+} \rightarrow C_{60-2n+2}^{z+} + C_2$ is statistically partitioned between $C_{60-2n+2}^{z+}$ and C_2. We have used Haarhoff's approximation [3] to calculate $G^*(\varepsilon - E_0^n)$ and $N(\varepsilon)$, assuming vibrational frequencies of $C_{60-2n+2}^{z+}$ to be replaced by those of a neutral C_{60} reported by Schettino et al. [4]

The critical activation energies E_0^n in eq. (2) are taken from the binding energies of $C_{60-2n+2}^{z+}$ ($n = 1 - 5$) for reaction (1) in the literature [2,5]. We adopted the two sets of the binding energies of $C_{60-2n+2}^{z+}$, i.e. the sets for the TS-1 and TS-3 models. The TS-3 transition state is consistent with a large frequency factor in the Arrhenius relation which has been expected by a very large rotational partition function of C_2. The binding energies of C_{60}^{+}, for example, are 7.06 eV and 9.2 eV for TS-1 and TS-3, respectively.

Figure 1 shows the fractional abundance K_n for C_{60-2n}^{z+} ions with the TS-3 model as a function of the internal energy of the primary C_{60}^{z+} at 25 µs after photoionization of C_{60}. We defined the appearance internal energy $E_{RRKM}(n)$ for the formation of C_{60-2n}^{z+} as the internal energy of C_{60}^{z+} corresponding to $K_n =$ $0.03 K_n^{max}$. The values of $E_{RRKM}(n)$ determined from Fig. 1 are listed in the seventh and eighth columns of Table 1. For the formation of C_{58}^{z+}, C_{56}^{z+}, and C_{54}^{z+} $E_{RRKM}(n)$ are 40.9, 47.0, and 52.8 eV, respectively, in excellent agreement with the observed maximum internal energies $E_{max}(1,z)$, $E_{max}(2,z)$, and $E_{max}(3,z)$, respectively. These results are the manifestation of the validity of the present statistical treatment: large amounts of the internal energy of C_{60}^{z+} is equilibrated among the vibrational degrees of freedom, and subsequent fragmentation proceeds through reaction (1) via a transition state with the activation energy of E_0^n.
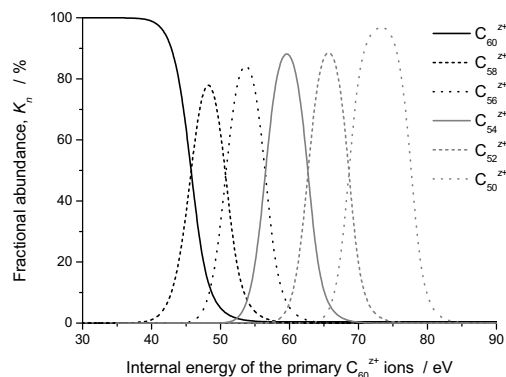
Fig. 1. Fractional abundance curves of C_{60}^{z+} and C_{60-2n}^{z+} ions obtained by using the RRKM theory (TS-3 model).

[1] R. K. Yoo *et al*., J. Chem. Phys. **96** (1992) 911.

[2] R. Wörgötter *et al*., J. Chem. Phys. **104** (1996 1225.

[3] W. Forst, *Theory of Unimolecular Reactions*, Chap. 6, Academic, New York, (1973).

[4] V. Schettino *et al*., J. Chem. Phys. **101** (1994) 11079.

[5] M. Foltin *et al*., J. Chem. Phys. **98** (1993) 9624.

Table 1   Upper limit $E_{max}(n,z)$ of the internal energies (eV) of the primary C_{60}^{z+} ions above which $C_{60-2n+2}^{z+}$ fragments cannot escape from further dissociating into $C_{60-2n}^{z+} + C_2$ ($n \geq 1$).

	$C_{60-2n+2}^{z+}$	C_{60-2n}^{z+}	Observed,[a] $E_{max}(n,z)$			Calculated,[b] $E_{RRKM}(n)$	
			$z = 1$	$z = 2$	$z = 3$	TS-1[c]	TS-3[d]
1	C_{60}^{z+}	C_{58}^{z+}	39.7±1	39.3±1	40.7±1	40.1	40.9
2	C_{58}^{z+}	C_{56}^{z+}	44.7±1	44.3±1	49.7±1	47.1	47.0
3	C_{56}^{z+}	C_{54}^{z+}	51.7±1	50.3±1	-	52.9	52.8
4	C_{54}^{z+}	C_{52}^{z+}	-	58.3±1	-	58.9	59.1
5	C_{52}^{z+}	C_{50}^{z+}	-	64.3±1	-	65.1	65.3

[a] Obtained from the appearance photon energies for the formation of C_{60-2n}^{z+} from C_{60}.
[b] Appearance internal energies of C_{60}^{z+} corresponding to $K_n = 0.03 K_n^{max}$ at 25 µs after photoionization of C_{60}. The RRKM theory is employed to derive the rate constant for reaction (1) from which the K_n curves can be calculated.
[c] $E_{RRKM}(n)$ determined from a set of the binding energies for the TS-1 model was employed.
[d] $E_{RRKM}(n)$ determined from Fig. 1. A set of the binding energies for the TS-3 model was employed.

Site-Specific Photoionization of Free Krypton Clusters

T. Hatsui[1], H. Setoyama[1], N. Kosugi[1], B. Wassermann[2], I.L. Bradeanu[3], E. Rühl[1,3]

[1]*Institute for Molecular Science, Okazaki 444-8585 Japan*
[2]*Institut für Experimentalphysik, Freie Universität Berlin, 14195 Berlin, Germany*
[3]*Institut für Physikalische Chemie, Universität Würzburg, 97074 Würzburg, Germany*

Cluster formation is known to give the decrease in binding energy, which is commonly interpreted in terms of final state polarization screening [1]. From earlier near-edge spectroscopy [2] it is known that the most significant changes in electronic structure are found in the regime of small clusters. In the present work, we investigate Kr 3d photoionization for variable size Kr clusters in the average size regime $<N> \leq 30$.

The experimental setup consists of a continuous supersonic jet expansion. The correlation between the expansion conditions and $<N>$ is taken from Karnbach et al. [3]. The jet is intersected with a beam of linearly polarized soft X-rays from the in-vacuum undulator beam line BL3U with an energy resolving power $E/\Delta E$ of $\sim 2 \times 10^3$ at 140 eV photon energy. Electrons are analyzed at 55° to the electric vector of the incident x-rays by a Scienta SES-200 electron spectrometer (path energy: 75 V).

The new features arising from cluster formation are observed at the binding energy lower than the bare atomic peaks. The cluster spectra are obtained by subtracting the atomic portion (Fig. 1). Subtraction of the atomic component from the raw spectra was only done until spectral distortions occurred because a dimer component of weak intensity exists near the atomic lines. This is consistent with the dimmer binding energy predicted by *ab initio* theoretical calculations, which is so close to the bare atomic one that the dimer components with small mixing ratio are invisible in the raw spectra. Core ionization energies calculated by using a simple model in combination with a phenomenological model, that describes perfect and defect cluster shapes, is shown at the top of Fig. 1.

We have performed a spectral de-convolution of these components by using identical Voigt profiles, which are evaluated from the atomic spectrum observed at the same instrumental condition (Lorentzian width: 93 meV [4], Gaussian width: 163 meV). The dimer- and the edge-components show no or little size effects. When the atomic profiles are used, then the two other ones (corner and face/bulk) do not give rise to a significantly different line shape, as verified by the experimental spectra. This allows us to fit the spectra with four components for each spin-orbit component (Fig. 1). The spectrum for $<N>=4$ consists of three surface components besides the dominant dimer. The smallest of these shifts is due to the corner sites of small clusters, followed by edge-, face-/bulk-sites. We note that face- and bulk-sites cannot be clearly distinguished from each other since their 3d ionization energies occur in the same energy regime (Fig. 1). As $<N>$ is increased one observes the following systematic changes in the spectra shown in Fig. 1. (i) The dimer component decreases substantially in relative intensity. Any shift is hardly observable and the different energy positions are well observable within the error limit; (ii) Corner-sites show an increasing shift reaching up to ~ -500 meV. The relative intensity of this component remains almost constant; (iii) Edge-sites gain substantially intensity, which is accompanied by a slight energy shift; (iv) Face-/bulk-sites also gain intensity and there is also a slight size dependence of this component. The model calculations show that substantially larger shifts occur for the bulk component, if large clusters are formed. This is in full agreement with recent experimental results [5]. The present work has successfully revealed size and site-specific Kr 3d ionization energies of considerably smaller clusters.
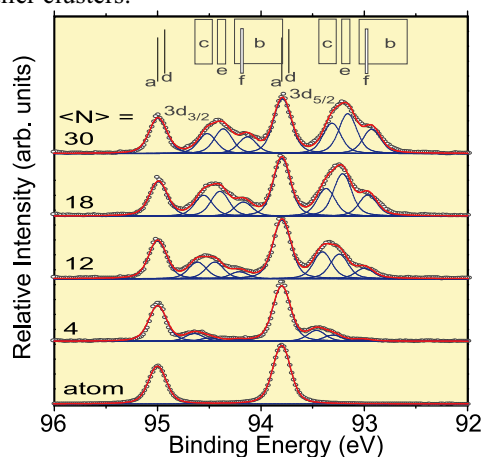
Fig. 1   Kr 3d photoelectron spectra of Kr clusters (○). The sum (−) of the spectral components (−) are given. The calculated energy regimes of different sites (a: atom, d: dimer, c: corner, e: edge, f: face, b: bulk) are shown at the top.

[1] O. Björneholm *et al*., J. Chem. Phys. **104** (1996) 1846.
[2] O. Björneholm *et al*., Phys. Rev. Lett. **74** (1995) 3017. A. Knop *et al*., Phys. Rev. Lett. **80** (1998) 2302.
[3] R. Karnbach *et al*., Rev. Sci. Instrum. **64** (1993) 2838.
[4] M. Jurvansuu *et al*., Phys. Rev. A**64** (2001) 012502.
[5] M. Tchaplyguine *et al*., J. Chem. Phys. **120** (2004) 345.

Double Photoionisation processes in SF$_6$

P. Lablanquie[1], Y. Hikosaka[1], E. Shigemasa[1], T. Aoto[2], K. Ito[2]

[1]*UVSOR Facility, Institute for Molecular Science, Okazaki 444-8585 Japan*
[2]*Photon Factory, Institute of Materials structure Science, Tsukuba 305-0801 Japan*

Double photoionisation, that is removal of two valence electrons from a molecule by a single VUV photon can usually proceed by two different paths, that form similar dication final states:

$$\rightarrow M^+ + e_{1=InnerShell} \rightarrow \qquad (A)$$
$$h\nu + M \xrightarrow{\hspace{2cm}} M^{2+} + e_1 + e_2 \quad (B)$$
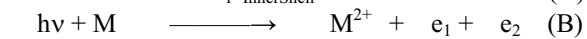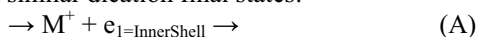
(A) is the Auger effect where an inner shell electron is first extracted and subsequent relaxation leads to emission of a secondary Auger electron. Valence double ionisation, (B) is often improperly referred to as 'direct double photoionisation', but includes in fact large contribution of indirect, sequential paths. It was recently demonstrated [1] that these indirect paths take surprisingly long time, with similar time scales for electron emission and nuclear motion, up to the point that the intermediate states often dissociate fully prior to emission of the second electron. We present here evidence of a different process in SF$_6$ molecules: an intense valence singly charged intermediate state autoionizes very efficiently through ICD (Inter Atomic Coulombic Decay [2]) prior to nuclear motion.

Experiment was performed on the new BL3U undulator line with the coincidence experimental setup developed at PF by Hikosaka *et al* [3]. Investigation of double photoionisation requires detection in coincidence of both emitted electrons, in order to define the reaction paths, which often means low signal. The trick in our experiment is to impose one of the two electrons to be of zero energy, and detect it with a threshold electron analyzer. Advantages are high collection-efficiency (on 4π sr) and potentially high energy-resolution.

Fig. 1 (bottom) displays the SF$_6$ L$_{2,3}$VV Auger spectrum. Its measurement in coincidence with the S2p$_{3/2}$ photoelectron (top) allows us to filter out the other S2p$_{1/2}$ spin-orbit Auger components, and to define precisely the final M^{2+} state and its binding energy (= photon energy minus the energetic electron energy). It is observed that the M^{2+} states populated by Auger decay are excited states, with the final 2 holes probably localized on the S atom, at the vicinity of the S2p hole. But experiment also reveals that M^{2+} states of lower binding energies can be accessed, with the 2 holes lying on F atoms [4]. These states are not populated by S2p Auger decay, and they can also be formed below S2p threshold as revealed in Fig. 2. Comparison with the non coincident photoelectron spectrum (in red) shows similar intensity profiles as the valence states of 40-45 eV binding energies, which are attributed to F2s hole states. The process is thus formation of F2s holes that decay rapidly through ICD mechanism [4]. This situation is specific to the SF$_6$ molecule, as usually intensity profiles are markedly different in photoelectron spectra and in e/e coincidence curves, as observed for N$_2$ in Fig. 2 (bottom).
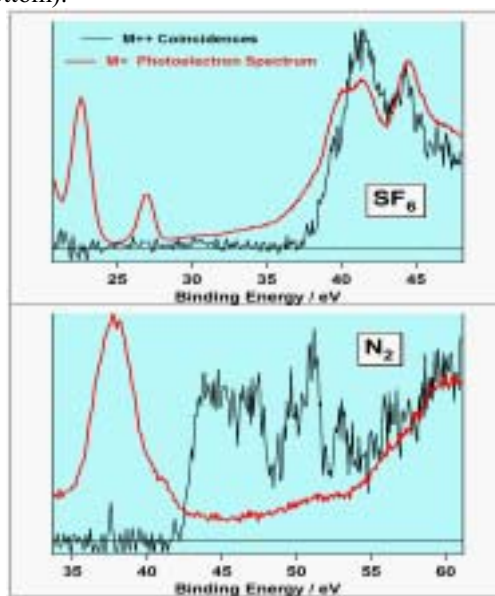
Fig. 2 Black: threshold electron / energetic electron coincidences measured with 80eV photons, and compared to the noncoincident photoelectron spectrum (red). Top: SF$_6$, Bottom: N$_2$.

Fig. 1 Bottom: SF6 Auger spectrum. Top: coincidence Auger spectrum measured at 2p$_{3/2}$ threshold.

[1] J. Eland *et al.,* Chem Phys **290** (2003) 27 and ref included.
[2] C. Buth *et al.,* J. Chem. Phys. **119** (2003) 10575.
[3] Y. Hikosaka *et al.,* Meas. Sci. Technol. **11** (2000) 1697.
[4] R. Feifel *et al.,* submitted to J. Chem. Phys.

Sub-Natural Linewidth Auger Electron Spectroscopy: Application to the Sulfur 2s Hole Decay in OCS

Y. Hikosaka[1], P. Lablanquie[1], E. Shigemasa[1], T. Aoto[2], K. Ito[2]

[1]*UVSOR Facility, Institute for Molecular Science, Okazaki 444-8585 Japan*
[2]*Photon Factory, Institute of Materials structure Science, Tsukuba 305-0801 Japan*

Inner-shell photoionization and the subsequent Auger decay give dication states as the final product. Since the kinetic energy of the Auger electron corresponds to the transition energy from the core-hole state to the dication state, spectroscopic information on the dication states is obtained by the analysis of individual Auger transitions. Auger spectroscopy has been, therefore, one of the most useful tools for investigating dication states. However, the analysis of Auger spectra has been restricted mainly for the following two reasons. First, the spectral features become complicated when the spectrum consists of the superposition of Auger lines associated with various core-hole states and their satellites. Second, the spectral resolution for an Auger line is limited by the natural width of the initial core-hole state.

Auger lines associated with a core-hole state can be distinguished by coincidence detection with the corresponding photoelectrons. Thus the difficulties resulting from the first restriction above can be removed by Photoelectron-Auger electron coincidence spectroscopy. Furthermore, this coincidence spectroscopy also enables the second restriction to be overcome and achieve a spectral resolution better than the natural width of the initial core-hole state. This sub-natural linewidth regime results from the complete definition of the dication states, brought about by the coincidences.

Detection of threshold photoelectrons, i.e. electrons with near-zero kinetic energy, takes advantage of the high energy-resolution (few meV) and high (4π) collection-efficiency that can be attained. These advantages are carried over to the Auger electron spectrum measured in coincidence, when we adopt threshold photoelectrons as the coincidence counterpart. So far, we have applied the threshold electron-Auger electron coincidence technique mainly to Auger transitions of rare gases, and have gained spectroscopic information on the dication states as well as the dynamics on the multiple ionization processes ([1] and references therein).

In this work, we have studied sulfur 2s decay in OCS using the threshold photoelectron-Auger electron coincidence technique. The S 2s hole has a very short lifetime resulting from the fast $L_1L_{2,3}V$ Coster-Kronig decay, and the resultant wide natural width (1.8 eV) has hidden the spectroscopic information on the final dication states. In practice, the Auger spectrum we measured with conventional Auger spectroscopy shows in the kinetic energy range 20-50eV only broad structures which can be allocated to the $L_1L_{2,3}V$ Coster-Kronig transitions (see Fig. 1(a)), and it is difficult to deduce the spectroscopic information on the dications from this spectrum. In contrast, the threshold photoelectron-Auger electron spectrum in Fig 1b exhibits the same dication states with a much higher energy resolution. Here, the energy resolutions of the Auger electron and threshold electron analyzers are set to around 0.8 eV and 30 meV (FWHM), respectively, and the photon energy band width is to 0.25 eV; therefore the energy resolution in the coincident spectrum is expected to be around 0.85 eV and the sub-natural linewidth regime is established by the coincidence measurement. Each structure in the coincidence spectrum is attributable to an electronic state with the configuration of (S 2p)$^{-1}$(valence)$^{-1}$, and their detailed interpretations are under way.
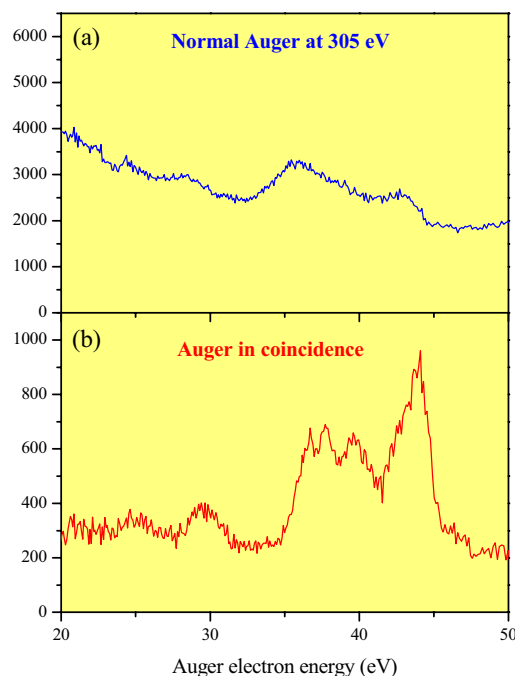
Fig. 1 (a) normal Auger electron spectrum measured at 305 eV photon energy. (b) Auger electron spectrum measured in coincidence with threshold photoelectrons at the S 2s threshold electron peak.

[1] F. Penent *et al*., J. Electron Spectrosc. Relat. Phenom. **144-147** (2005) 7.

Velocity Imaging Spectrometer for Negative Fragment Ions

Y. Hikosaka, E. Shigemasa

UVSOR Facility, Institute for Molecular Science, Okazaki 444-8585 Japan

Negative ion mass spectrometry working with synchrotron radiation source has been extensively used in investigation of the ion-pair formation, where negative ion detection achieves a basic discrimination against abundant photoionization processes associated with the formations of photoelectrons and positive ions. The negative ion yield curves have provided spectroscopic information on the superexcited states. Onsets in the curves often match the thermochemical thresholds for different ion-pair dissociation channels, from which one could deduce the states of the positive and negative ions formed. Ordinary mass spectrometry, however, rarely has the ability to determine kinetic energies and angular distributions of the fragment ions, though such information brings about further insights into the spectroscopy of the superexcited states and the dynamical property on the ion-pair dissociation.

We have developed a negative ion imaging spectrometer [1] designed to be used in combination with an ordinary synchrotron radiation source. The powerfulness of the imaging technique has been exerted on ion and photoelectron observations in the study of laser chemical dynamics. The advantages of the imaging technique applied to the study of the ion-pair formation process are (i) high collection efficiency (4π-sr. solid angle), and (ii) observation of the velocity vector distributions of fragment ions. The first useful information derived from the velocity vector distributions is the angular distribution with respect to the electric vector of the radiation. The angular distribution may imply the molecular orientation induced by photoexcitation, where the orientation reflects the symmetries of initially-formed superexcited states. The kinetic energy distribution of the negative fragment ions is the second useful information from the velocity vector distributions on image. Internal states of negative and positive fragments are accessible from the kinetic energy distribution. The electronic and ro-vibrational populations of the final fragments closely relate to the molecular states concerning the reaction dynamics.

The present negative ion imaging spectrometer is illustrated in Fig. 1. We have installed the imaging spectrometer on the beamline BL7B. The monochromatized synchrotron radiation has been introduced into the middle point between the plates P_1 and P_2 perpendicularly to the plane of Fig. 1. The polarization axis of light was positioned perpendicularly to the axis of the flight tube. Negatively-charged particles produced after photoabsorption, *i.e.* electrons and negative ions, can be extracted by the three-element electrostatic lens into the flight tube, and projected onto the position-sensitive detector terminating the tube. For observation of

negative ion images, we have applied a strong magnetic field in the ionization region, in order to suppress electrons' arrivals to the detector.

Usefulness of the present method for observing negative ions is clearly demonstrated on the images from O_2 measured at 21.06 eV photon energy with/without a strong magnetic field. The image observed without any extra magnetic field (Fig. 2(a)) is fully occupied by the electrons due mainly to the formations of O_2^+($b^4\Sigma_g^-$ and $B^2\Sigma_g^-$). In contrast, only a single ring due to O$^-$ fragments emerges in Fig. 2(b) as we applied the strong magnetic field. The single ring corresponds to the formation of O$^-$(^{2}P)+O$^+$(^{2}D). The intensity distribution along the circumstance of the ring shows that O$^-$ fragments are preferably emitted along the electric vector. This fact implies that the photoexcitation to Σ_u^- symmetry state(s) is dominant at this photon energy.
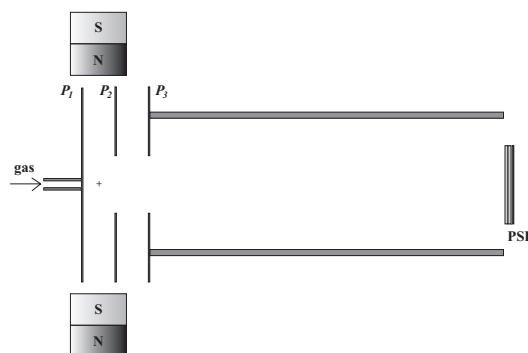
Fig. 1   A schematic view of the negative ion imaging spectrometer.
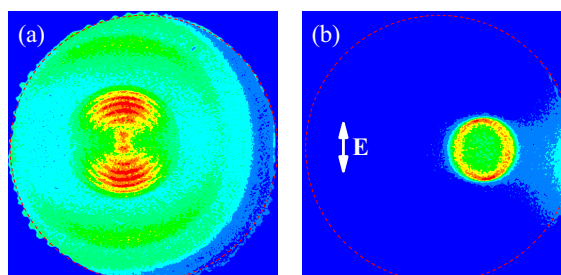
Fig. 2   Raw images from O_2 measured with 21.06 eV photons (a) without any extra magnetic field and (b) with a strong magnetic filed (~15 mT flux around the ionization region). Each image is plotted on an individual linear scale. The electric vector of the light lies along the vertical axis.

[1] Y. Hikosaka and E. Shigemasa, J. Electron Spectrosc. Relat. Phenom. **148** (2005) 5.

Negative Fragment Ion Formation from N_2O Studied by Velocity Imaging Spectroscopy

Y. Hikosaka, E. Shigemasa

UVSOR Facility, Institute for Molecular Science, Okazaki 444-8585 Japan

Formation of a pair of positive and negative fragment ions following molecular photoexcitation is commonly observed in the vacuum ultraviolet region, although in general this process occupies only a small fraction in the total cross section. The cross section of the ion-pair formation is often enhanced at superexcited states which are mostly Rydberg states converging to upper-lying ion states. The enhancements result from the interactions between the superexcited states and the ion-pair states correlating directly to ion-pair dissociation limits, and the interaction strength relates to the electronic properties and the potential energy surfaces of the relevant states. Accordingly the superexcited states indiscernable in the total cross section may be exhibited on the ion-pair formation; observation of the ion-pair formation, therefore, can be utilized as a specific probe for superexcited states.

We have developed a negative ion imaging spectrometer which uses magnetic field to filter out electron signals [1]. The present method enables us to perform imaging observation of negative ions, for the first time, by the use of ordinary synchrotron radiation which offers properties of wide tunability and linear polarization. We have applied the new method to ion-pair dissociation in N_2O, which proves and demonstrates the powerfulness of the present method in study on ion-pair dissociation dynamics.

Measurements were made at beamline BL7B. Formation of O^- fragments from N_2O is most extensive in the 18-20 eV photon energy range [2]. Figure 1 shows a total yield curve of the imaging detection. The spectral features on the yield curve are essentially equivalent to those on the O^- yield curve obtained by a quadrupole mass spectrometer [2], though the background due to remaining electrons is anticipated in the present curve. Five Rydberg series converging to $N_2O^+(C^2\Sigma^+)$ have been located in this photon energy range; though the assignments of the Rydberg series have been discussed, they are still not definitely determined. Two of the Rydberg series are remarkably exhibited in Fig. 1.

Negative ion images measured at five photon energies, two of which correspond to Rydberg peaks, are displayed in the inlets of Fig. 1. No clear ring can be seen on all the images, implying that the O^- fragments do not have some distinct kinetic energies but widely-distributed energies. Here, the kinetic energy distributions of the O^- fragments reflect the internal energy distributions of counterpart N_2^+ fragments, and accordingly the counterpart N_2^+ fragments are excited ro-vibrationally rather than only electronically. The excitation closely relates to the

shapes of the potential energy surfaces on which the ion-pair dissociation occurs. The images measured at non-resonant energies show weak preferences for the O^- emission in the perpendicular direction to the electric vector. In striking contrast, at the two resonant energies the O^- fragments are preferably emitted along the electric vector ($\beta=0.5$ at the lower resonance and $\beta=0.7$ at the higher one). This fact is a direct evidence that initial photoexciation to the two Rydberg states results from parallel transition, *i.e.* that the two Rydberg states have Σ symmetry, inconsistent with some previous interpretations inferred mainly from the quantum defects of the Rydberg states. The assignments we propose for these two Rydberg series are given in the figure.
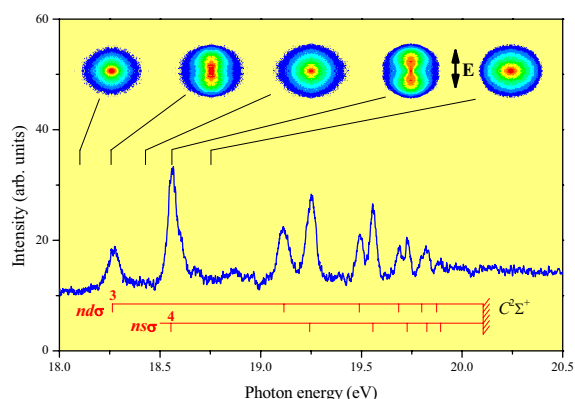
Fig. 1 A total yield curve of the imaging detection from N_2O photoionization with a strong magnetic field, which essentially corresponds to an O^- yield curve. Photon energy resolution is set to 20 meV. Energy levels of two Rydberg series converging to $N_2O^+(C^2\Sigma^+)$ are indicated with the assignments we propose. Raw O^- images measured at 18.10, 18.26, 18.43, 18.56 and 18.75 eV are attached. The electric vector of the light lies along the vertical axis.

[1] Y. Hikosaka and E. Shigemasa, J. Electron Spectrosc. Relat. Phenom. **148** (2005) 5.
[2] K. Mitsuke, S. Suzuki, T. Imamura and I. Koyano, J. Chem. Phys. **92** (1990) 6556.

Anisotropic Fragment Emission on Valence Photoionization of CF$_4$

Y. Hikosaka, E. Shigemasa

UVSOR Facility, Institute for Molecular Science, Okazaki 444-8585 Japan

As a prototype to understand photoionization dynamics of highly-symmetrical molecules, photoionization of CF$_4$ in the valence region has been studied extensively by both experiment and theoretical calculation. Photoabsorption spectra and electron energy loss spectra of CF$_4$ exhibit a few distinct features and are occupied mainly by broad structures. Harshbarger et al. assigned most of the structures to transitions into Rydberg orbitals [1], and their assignments have been accepted in several subsequent works. In contrast, Ying and Leung have ascribed the same structures to valence states associated with transitions to the unoccupied 5a$_2$ and 5t$_2$ orbitals [2].

Meanwhile, the partial photoionization cross sections and photoelectron asymmetry parameters measured for individual CF$_4^+$ states have been the most important experimental data to be reproduced by theoretical calculation. Although calculation results agree, to some extent, with the experimental curves, satisfactory interpretations are still not proposed to the physical origin of the modulations on the experimental curves. The most important and critical subject on the interpretations is again the transitions from each occupied orbital to the unoccupied 5a$_2$ and 5t$_2$ orbitals: the calculation results tend to put the transitions into the photoionization continua as shape resonances, in striking contrast to the assignments by Ying and Leung.

The present work offers new experimental information to understand dynamics on the CF$_4$ valence photoionization. Using the photoion velocity imaging method we have measured in hν=16-60 eV angular distributions of fragment ions with respect to the electric vector of light. The photoion images measured at hν= 17.4, 19.9, 29.9 and 46.5 eV are presented in Fig. 1. The photoion images correspond to projections of the initial three-dimensional photoion velocity distributions onto the detector. Here, the observed images are for all ion species, since the present imaging detection can not discriminate ion species. One would speculate that at every photon energy the isotropic fragment emissions result from the high symmetry (T$_d$) of the CF$_4$ neutral ground state; however, apparent anisotropy is practically observed on the fragment emissions at the lower three hν: the photoions at these photon energies are preferably emitted along the electric vector. The anisotropic fragment emissions directly imply that the initial molecular symmetry is broken on the dissciative photoionization.

Our interpretation to the origin of the observed anisotropies is as follows. Within the T$_d$ symmetry, the transition from an occupied orbital to one of the unoccupied orbitals should be isotopic with respect to

the electric vector and result in a triply-degenerated excited state with T$_2$ symmetry. Such a degenerated state is subject to symmetry distortion, and a T$_2$ state originally in T$_d$ symmetry results in an A$_1$ and E states after the distortion to C$_{3v}$. The dipole moment for the transition to the A$_1$ state is parallel to the C$_{3v}$ axis, while that for the transition to the E state is perpendicular to the axis. Here, the two transition moments are not necessarily the same any more after the symmetry distortion. Autoionization from such distorted excited states produces similarly-distorted CF$_4^+$ states. Since the CF$_4^+$(X, A) states have potential energy surfaces being repulsive associated with the C-F bond, the axis of the ion dissociation naturally coincides with the C$_{3v}$ axis. Photoexcitation to the A$_1$ and E states, therefore, promotes the positive and negative asymmetry with respect to the electric vector, respectively, for the resultant CF$_3^+$ fragments. The observed anisotropy is always positive, which implies that the parallel transition forming A$_1$ states is preferable to the perpendicular transitions. This may be reasonable, because both the 5a$_2$ and 5t$_2$ orbitals have the σ* character and the associated transitions have large contributions to the cross sections at the measured photon energies.
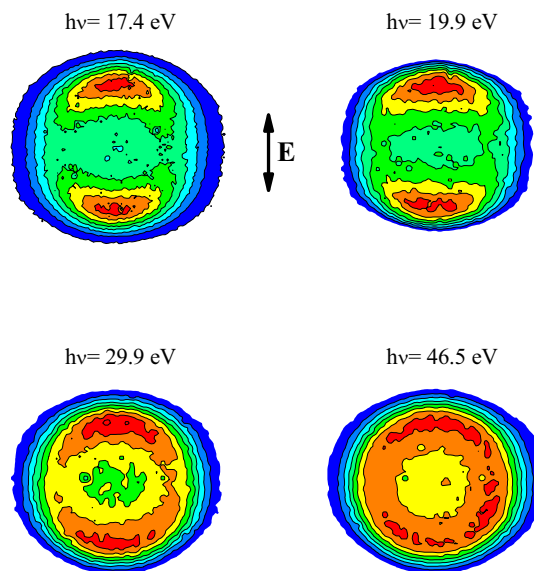
Fig. 1   Photoion images from CF$_4$ photoionization at hν=17.4, 19.9, 29.9 and 46.5 eV. Each image is plotted on an individual linear scale.

[1] W.R. Harshbarger *et al.*, J. Electron Spectrosc. Relat. Phenom. **1** (1972/1973) 319.
[2] J.F. Ying and K.T. Leung, J. Chem. Phys. **100** (1994) 7120.